JM3 Journal of Micro/Nanopatterning, Materials, and Metrology

RESEARCH PAPER

Diffraction-based overlay metrology using polarization-resolved dark-field digital holographic microscopy

Marc Noordam,[a,b,*] **Tamar Van Gardingen-Cromwijk**,[a,b] **and Arie den Boef**[a,b,c]

[a]Vrije Universiteit, LaserLaB, Department of Physics and Astronomy, Amsterdam, The Netherlands
[b]Advanced Research Center for Nanolithography (ARCNL), Amsterdam, The Netherlands
[c]ASML Netherlands B.V., Veldhoven, The Netherlands

ABSTRACT. **Background:** Accurate pattern positioning precision between two layers in a chip stack, known as an overlay (OV), is crucial in semiconductor device manufacturing. To facilitate the ongoing trend in the semiconductor industry to fabricate integrated circuits with smaller feature sizes, new dark-field OV metrology imaging systems are being investigated. A large challenge of dark-field microscopy is to correct the non-uniform intensity profile of the illumination beam.

Aim: We present a polarization-resolved dark-field digital holographic microscope to measure OV from the polarization response of diffraction-based OV (DBO) targets. It will be shown that polarization-resolved imaging of OV targets enables OV metrology that is robust against target position offsets and less sensitive to inhomogeneities in the intensity of the beam profile.

Approach: We retrieve the polarization response of the DBO target by simultaneously measuring the interference signals from two orthogonally polarized reference beams along with the image signal. The OV is retrieved from the polarization response of the $+1$st and -1st diffraction order.

Results: We experimentally demonstrate the OV-dependent first-order polarization response of a DBO target where the retrieved OV values remain independent of the target's position.

Conclusions: We present a polarization-resolved dark-field microscope for OV retrieval that remains robust for varying intensity profiles of the illumination beam.

 [DOI: 10.1117/1.JMM.24.1.014002]

Keywords: digital holographic microscopy; semiconductor overlay metrology; diffraction-based overlay; polarization; computational imaging

Paper 24081G received Oct. 21, 2024; revised Jan. 27, 2025; accepted Jan. 29, 2025; published Feb. 20, 2025.

1 Introduction

The ongoing trend in the semiconductor industry to fabricate integrated circuits with smaller feature sizes drives the need to improve metrology techniques. Accurate pattern positioning precision between two layers in a chip stack, called overlay (OV), is crucial in semiconductor device manufacturing, and diffraction-based overlay (DBO) metrology techniques are widely employed for precise overlay measurements. A DBO target consists of overlapping gratings that are located in two layers [see Fig. 1(a)]. The top grating is usually in photoresist, and the bottom grating is in an underlying product layer. The first reported DBO tools retrieved overlay from the 0th

*Address all correspondence to Marc Noordam, noordam@arcnl.nl

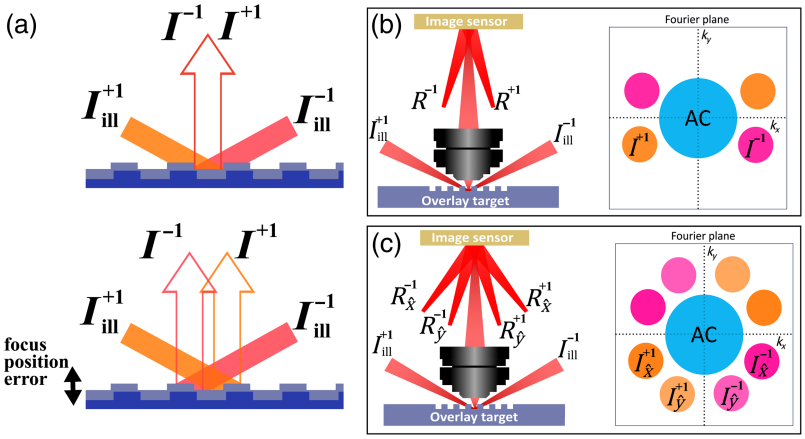

Fig. 1 Schematic overview of the OV detection using DBO target and DHM setup. (a) Depiction of diffracted +1st and −1st signals from a DBO target. In the bottom image, the target has a focus position offset leading to different locations of the illumination beams at the target. (b) Illustration of an intensity-based DHM setup where the +1st and −1st diffraction orders interfere with two separate reference beams under different angles. (c) Illustration of a polarization-based DHM setup where two reference beams with orthogonal polarization are used for both diffraction orders.

diffraction order.[1] However, using the 0th diffraction order requires eight overlapping grating pairs for an overlay measurement in the x and y directions. Moreover, 0th-order detection is sensitive to small intensity fluctuations and processing variations that may occur within an overlay target. For this reason, later DBO tools detect only the +1st and −1st diffraction orders.[2–5] To retrieve the OV, various optical setups have been developed to capture the +1st and −1st diffraction signals. A significant advancement in this field involves optical configurations that enable simultaneous retrieval of both diffraction order signals, effectively mitigating the impact of temporal fluctuations in the light source. Currently, available solutions include bright-field illumination setups, where the diffraction signals are allocated to specific regions of the Fourier spectrum. These signals can be separated by imaging the back focal plane of the objective onto a CCD array.

As circuit complexity continues to increase, overlay metrology demands robust sub-nanometer precision across diverse chip stack materials and thicknesses, often involving extremely thin films and requiring minimal surface area. To address these challenges, recent advancements have focused on employing specialized high-numerical-aperture (NA) objectives and leveraging multiple wavelengths. Dark-field digital holographic microscopy (df-DHM) builds on traditional DBO metrology techniques and has been proposed as a solution to meet the demands of OV metrology for increasingly complex circuits.[6–9] The dark-field imaging setup enables the full numerical aperture (NA) of the objective to be utilized for capturing diffraction signals while also accommodating large illumination angles, which makes it suitable for measuring small-pitch DBO targets. To measure the response of the +1st and −1st diffraction orders simultaneously, in df-DHM, the diffracted light generated by two illumination beams is imaged using a high-NA objective and interfered with two off-axis reference beams on the image camera, as sketched in Fig. 1(b). The interference signals from the diffraction orders, due to the different off-axis angles of the reference beams, have varying spatial frequencies depending on the angle of the reference beam. Employing digital fast Fourier transform (FFT) techniques for the computational selection of the distinct interference patterns yields the amplitude and phase information of both diffraction orders from which the OV is calculated. The retrieval of the full complex field (amplitude and phase) allows us to computationally correct for aberrations in the imaging system, as reported in Refs. 10 and 11. As the measured OV is derived from the measured intensities of the +1st and −1st diffraction orders, it depends on the intensity of the illumination beams. Therefore, to be robust against target position shifts in the measurement, the intensity profile of the illumination spot should ideally have a top-hat shape.

The demand to characterize compact DBO targets with small pitch sizes requires a high-NA imaging microscope, where the illumination beams have a large angle of incidence (~70 deg).

Due to the high-NA of the microscope objective, only low-NA lenses can be used for the illumination beams. The low-NA lenses for the illumination beams make it not feasible to create a small top-hat illumination profile at the target. Instead, a Gaussian illumination beam spot is produced. The Gaussian spot profiles of the illumination beams at a high angle lead to large variations in the illumination intensity at the target between the +1st and −1st illumination beams, which can result in OV errors when using intensity-based df-DHM. This issue can be addressed using larger spot sizes, albeit at the cost of photon efficiency, and by employing illumination correction schemes that utilize calibration measurements on a large grating.[12] However, when the DBO target is not measured at precisely the same focus position as the calibration grating, the effective spot profile locations differ due to the high incoming angles of the illumination beams. The dependence on the spot position of the illumination beams on the focus position of the target is illustrated in Fig. 1(a).

To overcome these issues and make the df-DHM technique independent of incoming intensity profiles in the +1st and −1st order illumination, we propose polarization-based rather than intensity-based OV retrieval using df-DHM. In polarization-based OV retrieval, the polarization response of the +1st and −1st diffraction orders is used for OV retrieval. As the polarization response is independent of the local intensity profiles of the illumination beams, polarization-based OV retrieval is unaffected by variations in the intensity profiles. Studies investigating the 0th-order DBO response have already demonstrated an OV dependency on the state of polarization.[13,14] This study will focus on the polarization response of the +1st and −1st diffraction orders, more similar to current intensity-based DBO techniques.

To retrieve the polarization response of a DBO target, the interference techniques used in intensity-based df-DHM, to simultaneously retrieve the two diffraction orders, can be further exploited. However, polarization-resolved df-DHM uses four reference beams at different angles of incidence, two orthogonally polarized reference beams for each diffraction signal [see Fig. 1(c)]. As the interference signal is a projection of the polarization of a reference beam with the imaged signal, two holograms are retrieved for each diffraction order signal, containing horizontal and vertical polarization information.[15–18]

In this paper, we experimentally demonstrate polarization-resolved OV retrieval using single-shot polarization extraction using a holographic microscope technique. First, the technical details of the polarization-resolved df-DHM setup will be discussed alongside a theoretical framework of the polarization response of the +1st and −1st diffraction orders of a DBO target as a function of OV. Later, we experimentally demonstrate OV retrieval from the polarization response of a DBO target and compare polarization-resolved OV retrieval with intensity-based illumination correction techniques. Finally, we measure OV as a function of target focus position, illustrating the benefits of polarization-dependent OV measurement compared with intensity-based df-DHM techniques.

2 Theory

This section describes the theoretical framework of polarization-resolved df-DHM DBO measurements. First, we briefly discuss how to retrieve OV information from the +1st and −1st order responses of DBO targets. Second, we address the correction for different illumination profiles. Finally, we derive polarization-resolved OV sensitivity.

2.1 Diffraction-Based Overlay

A DBO target consists of two gratings aligned in two different stack layers [see Fig. 1(a)]. The OV-dependent diffraction signal, R, has an opposite sign for the +1st and −1st diffraction orders and can be described as follows:[3,4]

$$R^{+} = I_{\mathrm{ill}}^{+}(\vec{r}) * \mathrm{DE}(1 + K * \mathrm{OV}) \quad \text{and} \quad R^{-} = I_{\mathrm{ill}}^{-}(\vec{r}) * \mathrm{DE}(1 - K * \mathrm{OV}). \tag{1}$$

Here, $I_{\mathrm{ill}}^{(\pm)}(\vec{r})$ represents the intensity profile at the spatial position, $\vec{r}$, on the target for the two spot profiles of the illumination beams. DE and K are target-specific parameters, where K is OV sensitivity and DE is the diffraction efficiency at zero OV. The OV value can be retrieved independent of the target-specific parameters DE and K by measuring two gratings with a known OV bias of $+d$ and $-d$ and using

$$\mathrm{OV} = d * \frac{A_{+d} + A_{-d}}{A_{+d} - A_{-d}}. \tag{2}$$

Here, A_{+d} and A_{-d} are the differences between the R^+ and R^- for the grating with an OV bias of $+d$ and $-d$, respectively

$$A_{\pm d} = R^+_{\pm d} - R^-_{\pm d}. \tag{3}$$

Equation (2) is valid for an arbitrary slope in A as a function of OV. However, an OV-independent offset in A introduces an error in the retrieved OV. Combining Eq. (1) with Eq. (3) gives

$$A = R^+ - R^- = 2(I^+_{\mathrm{ill}}(\vec{r}) + I^-_{\mathrm{ill}}(\vec{r})) * K * \mathrm{DE} * \mathrm{OV} + 2(I^+_{\mathrm{ill}}(\vec{r}) - I^-_{\mathrm{ill}}(\vec{r})) * \mathrm{DE}. \tag{4}$$

From Eq. (4), it follows that if $I^+_{\mathrm{ill}}(\vec{r})$ is equal to $I^-_{\mathrm{ill}}(\vec{r})$, A has zero offset with respect to OV. However, a difference in the intensity distribution of the illumination beams creates an OV-independent offset in A and can lead to an inaccuracy in the retrieved OV.

2.2 Illumination Profile Calibration

As df-DHM uses two separate oblique illumination beams for the $+1$st and -1st diffraction order, their illumination profiles are not necessarily equal. Equation (2) is only valid if A is a linear function with zero offset and an illumination intensity distribution difference creates an offset in A according to Eq. (4).

The illumination intensity distribution difference can be corrected using a calibration measurement on a large grating with equal diffraction efficiencies for $+1$st and -1st orders.[12] The first-order diffraction intensity signals of a calibration sample can be described as

$$R^\pm_{\mathrm{corr}} = I^\pm_{\mathrm{ill}}(\vec{r}) * \mathrm{DE}_{\mathrm{corr}}. \tag{5}$$

Dividing the measured intensity of the DBO target by the measured intensity of the calibration sample for each diffraction order removes the dependency on the illumination spot profiles

$$\frac{R^\pm_{\mathrm{target}}}{R^\pm_{\mathrm{corr}}} = \frac{\mathrm{DE}}{\mathrm{DE}_{\mathrm{corr}}} * (1 \pm K * \mathrm{OV}). \tag{6}$$

This method requires that the illumination intensity distribution on the target matches the intensity distribution on the calibration grating. If both samples are positioned at the same target location, this condition can be assumed to be met. However, even slight deviations from the intended focus position can result in differences in intensity profiles due to the high incoming angle of the illumination beams, see Fig. 1(a). Furthermore, if the top and bottom gratings of a DBO target are not perfectly aligned but instead have a lateral spacing between them, the illumination profiles for the top and bottom gratings will differ. This discrepancy leads to uncorrectable errors in the retrieved OV.

2.3 Polarization-Resolved df-DHM

In polarization-resolved df-DHM, the horizontal and vertical polarization components of both the $+1$st and -1st order are simultaneously measured, leading to four response signals

$$R^\pm_h = I^\pm_{\mathrm{ill},h}(\vec{r})\mathrm{DE}_h(1 \pm K_h * \mathrm{OV}) \quad \text{and} \quad R^\pm_v = I^\pm_{\mathrm{ill},v}(\vec{r})\mathrm{DE}_v(1 \pm K_v * \mathrm{OV}). \tag{7}$$

Here, DE_h, DE_v, K_h, and K_v are the polarization-dependent stack parameters. The illumination intensity distribution is equal for the horizontal and vertical polarization components, so

$$\frac{|E^\pm_{\mathrm{ill},v}(\vec{r})|}{|E^\pm_{\mathrm{ill},h}(\vec{r})|} = p^\pm. \tag{8}$$

Here, $p^\pm$ represents the scaling factor between the polarization states of the illumination beams that is independent of the position $\vec{r}$. Dividing the intensity response of the two polarization components for $+1$st and -1st order gives

$$\frac{R_v^{\pm}}{R_h^{\pm}} = (p^{\pm})^2 \frac{\mathrm{DE}_v(1 \pm K_v * \mathrm{OV})}{\mathrm{DE}_h(1 \pm K_h * \mathrm{OV})} \approx (p^{\pm})^2 \frac{\mathrm{DE}_v}{DE_h}(1 \pm (K_v - K_h) * \mathrm{OV}). \tag{9}$$

Here, we use the Taylor approximation, assuming that $DE \gg K * OV$ in DBO targets. The right-hand term in Eq. (9) is similar to Eq. (1) but is not dependent on the illumination intensity distribution.

3 Method

A schematic of the polarization-resolved df-DHM setup is shown in Fig. 2. A supercontinuum source generates broadband light, which is subsequently filtered by an acousto-optic tunable filter (AOTF) and a bandpass filter to produce laser light with a central wavelength of 647 nm and a bandwidth of ~2 nm. This bandwidth results in a coherence length that is sufficiently large to maintain interference between the object and reference beams across the field of view, whereas the coherence length is short enough to make the +1st and −1st order beams mutually incoherent by creating a deliberate optical path difference between the +1st and −1st order beams.[19] Note that a supercontinuum laser source in combination with an AOTF can achieve wavelength switching across a broad wavelength range, which can be advantageous for OV metrology applications[2] because OV sensitivities for a specific DBO target are wavelength-dependent.[9] In this study, the wavelength was selected based on the available range of our AOTF and the compatibility with the available bandpass filters. The laser beam is split into two equal parts for the +1st and −1st beam path using a 50:50 non-polarizing beam splitter. The beam paths for the two diffraction orders are identical except for their optical path lengths, ensuring that the diffraction orders are not coherent with each other.[8] For each diffraction order, the beam is split into a reference and an illumination branch using a 90:10 ($R:T$) non-polarizing beam splitter.

In the reference branch, a polarizing beam splitter separates the horizontal and vertical polarization components. Two mirrors adjust the position and angle of one of the polarization components before the paths of the different polarization components are recombined using a polarizing beamsplitter. This ensures that both polarization components of the reference beam reach the image sensor at the same position but with different angles of incidence. A delay line is used to make both polarization components of the reference beams temporally coherent, and two lenses are used to focus both reference beams at a distance d from the image sensor. This distance matches the distance from the objective to the image plane,[8] expanding the beam profile of the reference beams to the size of the image sensor and generating a quadratic phase front similar to the one produced by the objective.

The two illumination branches also contain a tunable delay line to accurately match the optical path distance between the reference and illumination beams. The intensity and the linear

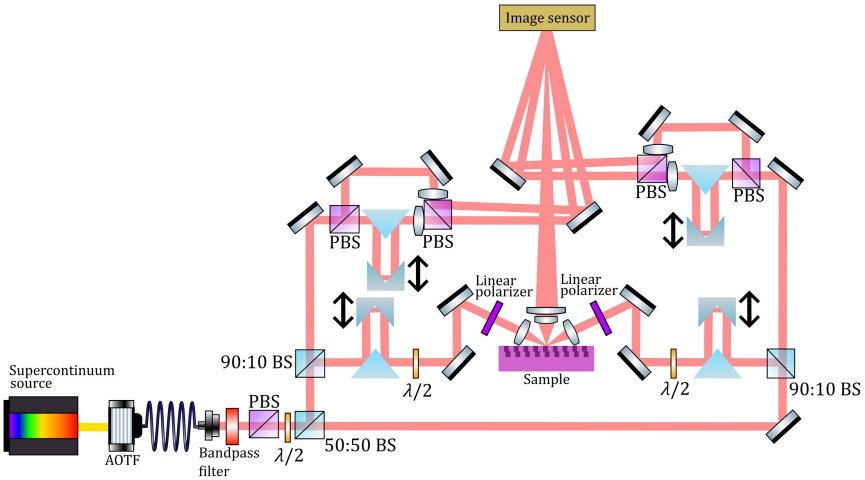

Fig. 2 Sketch of the optical setup.

polarization angle of the illumination beams are set using a half-wave plate in combination with a Glan–Taylor linear polarizer. The polarization angle of the illumination beams is set at 45 deg to ensure equal intensity for both polarization components. Finally, the illumination beam is focused by a lens with a focal length of 50 mm on the sample surface at the 70-deg angle of incidence, resulting in an elliptical beam profile at the target with an full width half maximum (FWHM) of 30 μm in the x direction and an FWHM of 10 μm in the y direction. The illumination beams have a horizontal plane of incidence that is perpendicular to the vertically oriented grating ridges.

In this paper, we utilize DBO targets located on a calibration wafer designed for DBO methods, fabricated through a mature process suitable for industrial applications, which ensures a technical OV margin below 2 nm. The diffracted light from the DBO target is collected by a custom-made imaging objective manufactured by Anteryon, which consists of two lens elements, identical to the one described in Ref. 11. The objective lens with an NA of 0.8 and a focal length of 7.2 mm directs the light to the image sensor placed ~720 mm from the objective to image the sample with a roughly 100 times magnification. The image sensor is a CMOS camera (Basler A2A4504-27g5mBAS, Ahrensburg, Germany) with a 4504×4504 pixel array and a square pixel size of 2.74 μm.

The digital reconstruction of the four holograms from a measured interference pattern with the polarization-resolved df-DHM microscope is shown in Fig. 3. Here, the first-order diffraction signals of a DBO target are imaged. The DBO target consists of two square grating patterns with a programmed OV offset of $d = \pm 20$ nm. The individual gratings have a width of 8 μm and a grating pitch of 600 nm, ensuring that the diffracted signal is approximately perpendicular to the target. Both the diffraction orders separately interfere with two off-axis orthogonally polarized reference beams, resulting in a measured intensity pattern with four spatial frequencies, as shown in Fig. 3(a). The intensity of the reference beams is measured separately and subtracted from the interference signal to improve the measurement signal.

Next, a 2D FFT is calculated from the measured interference signal, as shown in Fig. 3(b). In the Fourier domain, the four distinct spatial frequencies corresponding to the four holograms are well separated. The intensity profile of the separate holograms in the Fourier domain illustrates the intensity distribution in the back focal plane of the microscope objective. From the inset in Fig. 3(b), a double 2D sinc function originating from the square grating structures of the DBO target can be observed. To calculate the response of the individual holograms at the image plane, the holograms are separately filtered in the Fourier domain, and the relevant sidebands of each hologram are shifted to the center of the Fourier domain. Calculating the 2D inverse FFT of the four filtered signals results in four holographic images that contain the complex field information of the diffraction response from the DBO target. Finally, the holograms are divided by the square root of the intensity signal of their respective reference beam.

In Fig. 3(c), the calculated intensities from the four holographic images are plotted. Although the intensity response should be uniform over the full grating structure of the OV

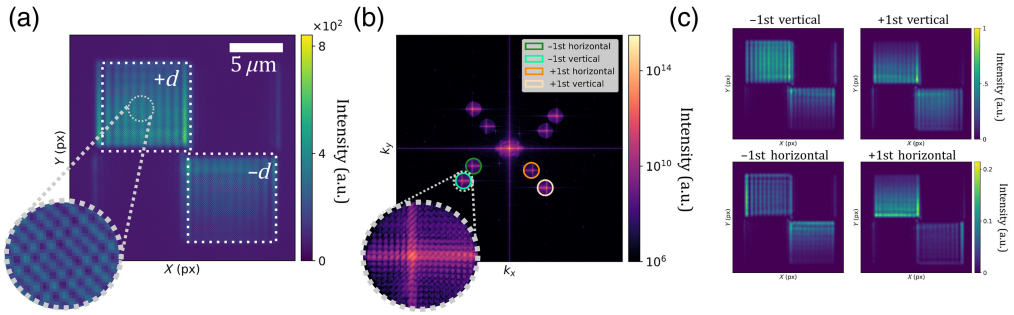

Fig. 3 Digital reconstruction of the four holograms from the measured interference pattern. (a) Measured intensity of the interference pattern generated from the four off-axis reference beams and the image of a DBO target consisting of two square gratings with a programmed OV value of $d = +20$ and $d = -20$. (b) Fourier plane of the measured interference patterns. The holograms are well separated due to their different spatial frequencies. (c) The calculated intensities of the four reconstructed holograms obtained by filtering in the Fourier domain.

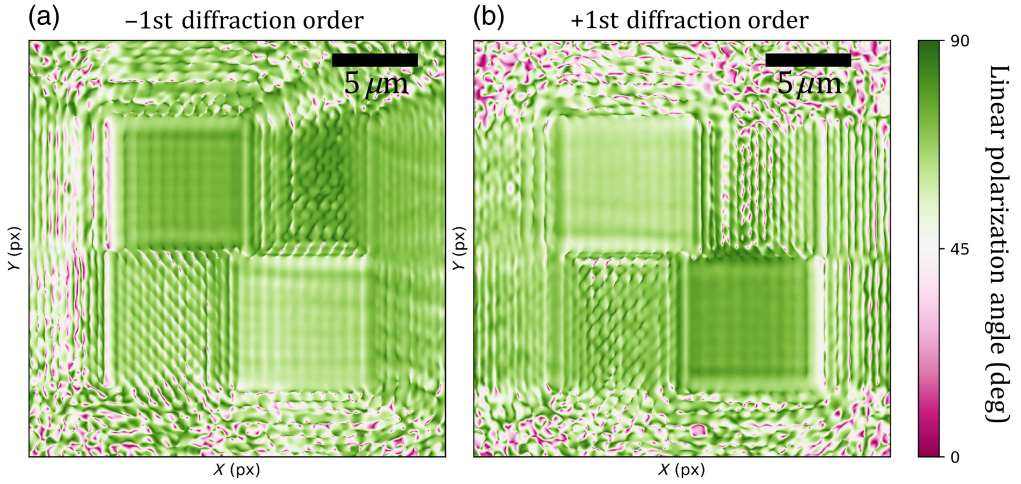

Fig. 4 Measurement of the linear polarization response of a DBO target for the +1st and −1st diffraction order. The linear polarization angle is obtained using Eq. (10) for the −1st (a) and +1st (b) diffraction order.

targets, Fig. 3(c) shows that the measured intensity fluctuates across the grating structures. These intensity fluctuations are caused by the intensity profile of the illumination beam. As the spot sizes of both illumination beams are roughly the same as the target, the illumination intensity fluctuates over the grating structures, causing variations in the measured diffracted light. For OV retrieval using Eq. (2), the intensity variations over the DBO target can lead to significant OV errors.

The linear polarization angle of the DBO target, α, of the diffraction response can be calculated from the retrieved holograms using the following equation:

$$\alpha^{(+,-)} = \tan^{-1}\left(\frac{|E_{\text{vertical}}^{(+,-)}|}{|E_{\text{horizontal}}^{(+,-)}|}\right). \tag{10}$$

In Fig. 4, the linear polarization angle is plotted for the +1st and −1st diffraction orders. The intensity response of the individual polarization components used to retrieve the polarization angle [as shown in Fig. 3(c)] exhibits significant variation across the DBO target. However, from Fig. 4, it can be observed that the polarization angle response is uniform across the two gratings of the DBO target, with polarization signal fluctuations within the pads being smaller than the differences between the pads. The flat response of the polarization angle can be explained by the equal spot-profile illumination for both polarization components. Further details on the polarization angle of illumination beams can be found in the Appendix (Fig. 8). Therefore, dividing the response of the two polarization components in Eq. (10) eliminates the error introduced by fluctuating illumination intensity.

Furthermore, Fig. 4 shows that the polarization response of the grating with a programmed OV offset of $d = 20$ nm (a) is different from the polarization response of the grating with a programmed OV offset of $d = -20$ nm (b). This effect indicates that, in addition to a general polarization rotation of the DBO targets from the initial polarization angle of 45 deg, there is also an OV-dependent polarization rotation. The polarization angle rotation shows a symmetric response over the different diffraction orders. Specifically, the +1st order polarization response of the $-d$ grating is equal to the −1st order polarization response of the $+d$ grating and the −1st order polarization response of the $+d$ grating is equal to the +1st order polarization response of the $-d$ grating.

4 Results

In this section, we compare the robustness of OV retrieval in the presence of small focus variations using three different methods. The first method is intensity-based with no illumination

correction. In this case, an intensity difference between the +1st and −1st order illumination profiles directly influences the OV retrieval. The second method is intensity-based, where the illumination beams' spot profiles are corrected using a calibration measurement on a large grating, as described in Ref. 12. The illumination beam spot profiles are correctly compensated if the calibration grating and the DBO target have the same focus position. The third method uses polarization-resolved df-DHM. Here, the response of the horizontal and vertical polarization components is divided, as described in Eq. (9). In this method, OV is intrinsically independent of the illumination spot profiles for every focus position of the target.

Figure 5 shows the intensity difference between the +1st and −1st order signal, A, for the three methods mentioned above. The two grating structures of the DBO target have a nominal overlay of 0 nm and a bias d of $+20$ and -20 nm. In Fig. 5(a), the intensity-based difference signal, A, without illumination correction is plotted. Here, it can be observed that the intensity difference between the +1st and −1st order images varies over the grating due to the intensity differences of the illumination spot profiles. Therefore, OV retrieval without illumination correction would be unreliable using the df-DHM setup demonstrated in this paper. In Fig. 5(b), the intensity-based illumination-corrected intensity difference is plotted. A constant signal over the gratings can be observed, with the two gratings having opposite programmed OV values clearly showing opposite signals. In Fig. 5(c), the polarization-resolved OV is plotted. Similar to the illumination calibration method, polarization-resolved df-DHM shows a flat response over the gratings with an opposite value for the two gratings. However, for polarization-resolved df-DHM, no calibration measurement is needed to correct the spot profiles of the illumination beam.

Next, we investigate the OV response for multiple DBO targets with different set OV values. Figure 6 shows the retrieved OV as a function of the programmed overlay for the three different methods. In Fig. 6(a), the retrieved OV values of the intensity-based method without illumination correction are plotted. Here, no correlation between the programmed and retrieved OV values can be observed. For the illumination calibration and polarization-resolved methods, a clear correlation between the programmed and retrieved OV values can be observed in Figs. 6(b) and 6(c), respectively. A linear fit through the data points provides the slope and offset values of the retrieved OV curve. The linear fits shown in Fig. 6 indicate that the slope and offset values slightly deviate from the ideal values of 1 and 0, respectively. This can be explained by the impact of differential asymmetry of the illumination polarization state, further described in the

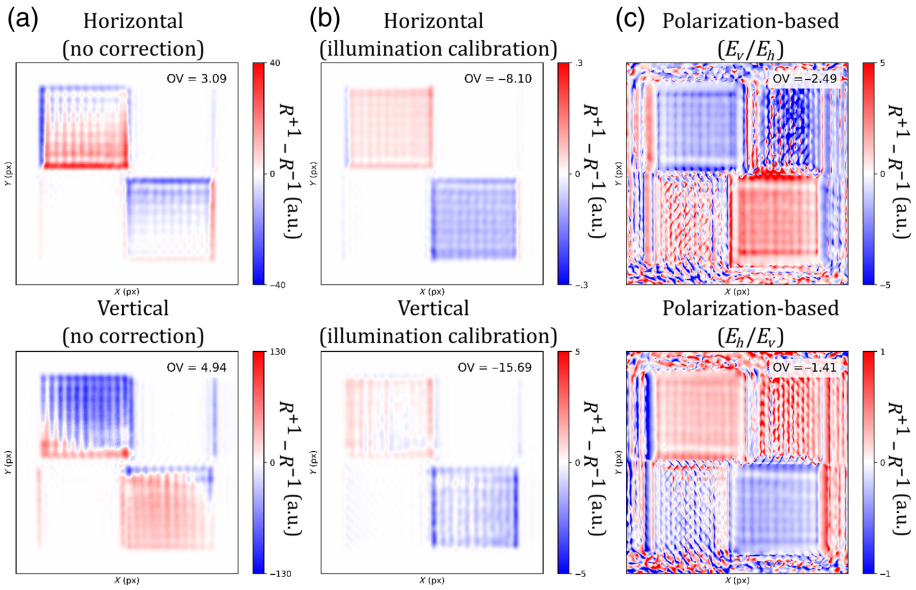

Fig. 5 Intensity difference between the +1st and −1st order signal at a DBO target consisting of two square gratings with programmed OV values of $d = 20$ nm and $d = -20$ nm. Three different illumination correction methods are used: no illumination correction (a), illumination correction using a calibration grating (b), and polarization-resolved correction (c).

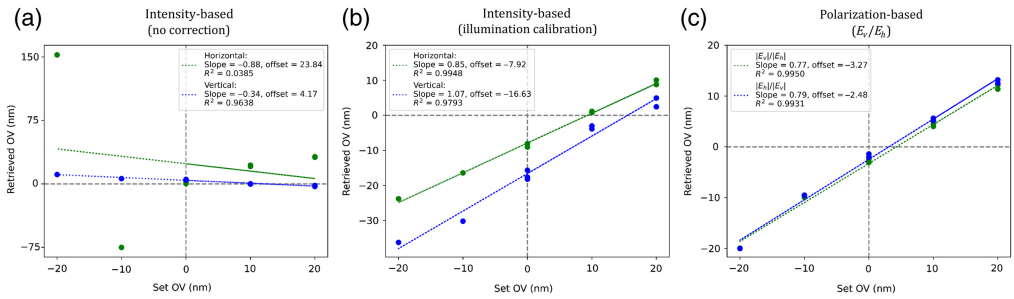

Fig. 6 Retrieved OV plotted as a function of the programmed OV of multiple DBO targets. Three different illumination correction methods are used: no illumination correction (a), illumination correction using a calibration grating (b), and polarization-resolved correction (c). The dotted lines depict linear fit through the data points, from which the slope and offset of the OV curves are extracted.

Appendix. From the insets of Fig. 6, it can be observed that the correlation coefficients (R^2) are similar for the illumination calibration and polarization-based methods, indicating comparable performance in this measurement set. However, achieving a robust and precise focus on the target in real-world applications can be challenging. In such cases, polarization-based OV retrieval is significantly less dependent on focus correction compared with the intensity-based method, as we will elaborate on in the following paragraph.

Due to the high angle of incidence of the illumination beams, their intensity profile changes as a function of the target defocus. To investigate the effect of target-position errors on the retrieved OV, the OV is measured as a function of the target's focus position. Figure 7 shows the retrieved OV of a DBO target with a programmed overlay of 0 as a function of the target's focus position. The retrieved OV values are normalized at the zero-target focus position. Here, the intensity-based method with illumination correction is compared with the polarization-resolved method. From Fig. 7, it can be observed that with intensity-based retrieval, the retrieved OV values vary by several nanometers for a target focus shift of only 2 μm. However, using the polarization-resolved method, the retrieved OV values remain constant as a function of the target's focus position. The plot in Fig. 7 demonstrates the independence of the polarization-resolved df-DHM method compared with intensity-based techniques.

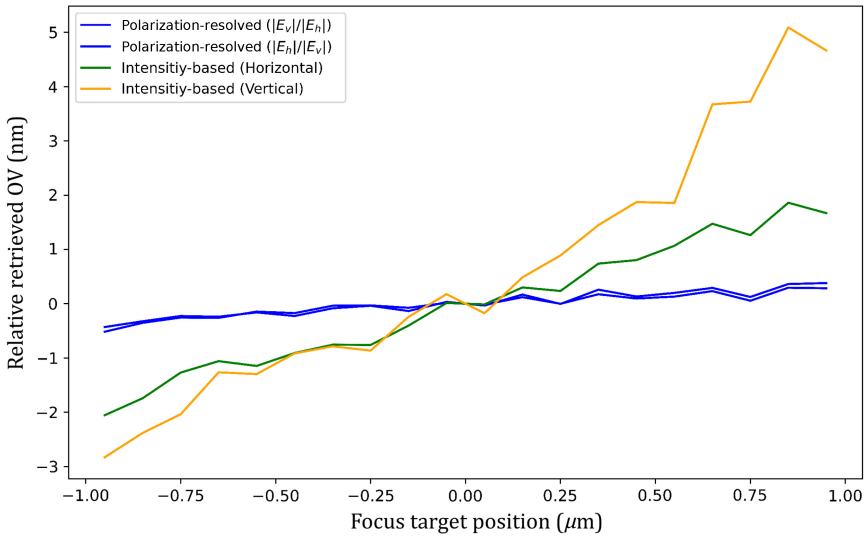

Fig. 7 Retrieved OV as a function of the focus position of the target. The retrieved OV values are normalized at the zero focus position of the target.

5 Discussion and Conclusion

Spatial intensity fluctuations of the illumination beam can directly cause imaging errors in dark-field microscopy. In high-precision metrology applications, such as OV metrology, these imaging errors result in inaccurate measurements. In this paper, we demonstrate a polarization-resolved dark-field microscopy technique that is independent of illumination beam intensity fluctuations. Importantly, in this method, the polarization components are measured simultaneously to circumvent measurement errors caused by temporal fluctuations of the laser source. This work illustrates the advantages of polarization-resolved dark-field digital holographic microscopy for a real-world application known as OV metrology. Here, we have demonstrated that OV retrieval using polarization-resolved df-DHM is particularly robust against position errors of the DBO target. Polarization-resolved df-DHM shares a similar application domain with regular DBO methods, where challenges such as local tilt variations caused by bow and warp can persist. However, by utilizing the DHM method to retrieve the pupil field, advanced computational techniques can be further explored to mitigate these effects.

Polarization-resolved df-DHM can be further explored in microscopy applications with an ill-defined or rapidly varying illumination beam profile, where characterizing the spot profiles of the illumination beam is difficult. Specifically, in OV metrology, polarization-resolved df-DHM can be useful for thick-stack DBO targets with a large separation between the top and bottom gratings. For example, in emerging applications such as die-to-wafer hybrid bonding techniques, a relatively long coherence length—on the order of several hundreds of micrometers—is required. This can be achieved by selecting sufficiently narrowband light with a bandwidth of ~1 nm. In addition, the need to penetrate silicon drives the use of longer wavelengths, taking advantage of silicon's transparency in those spectral regions. In thick-stack DBO targets, the illumination intensity beam profiles differ for the top and bottom gratings due to the high incoming angles, making illumination correction impractical; however, polarization-resolved OV retrieval is still possible. Additional investigation into the polarization-resolved OV sensitivity of different DBO targets could be beneficial in future work, particularly by exploring alternative setup configurations to address challenges such as low OV sensitivity in one polarization direction. For example, employing conical diffraction with a target grating oriented at a 45-deg angle may offer potential improvements.

Finally, polarization-resolved df-DHM can also solve challenges inherent to holographic microscopy. For instance, high-frequency sample vibration can lead to phase wash-out of the interference signal, resulting in a smaller retrieved signal amplitude.[20] As both polarization components experience a similar phase wash-out effect, the polarization state is not affected by sample vibrations.

6 Appendix: Impact of Differential Asymmetry of the Illumination Polarization State

Ideally, the polarization state, $p^{\pm}$, of the two illumination beams is independent of the position $\vec{r}$ within the illumination spot. However, a small variation of $p^{\pm}$ was observed across the illumination spot, which we attribute to small imperfections in the optics of our test setup, as can be observed in Fig. 8. In the inset of Fig. 8, we calculate the average polarization signal for the regions of interest corresponding to the size and location of the DBO target pads. As a result, the $+d$ and $-d$ pads of the overlay target experience slightly different asymmetry offsets ($\Delta A_{\pm d}$) in the measured asymmetry ($A_{\pm d}$) of the polarization state of the $+d$ and $-d$ pads

$$A_{+d} = K * (\mathrm{OV} + d) + \Delta A_{+d} \quad \text{and} \quad A_{-d} = K * (\mathrm{OV} - d) + \Delta A_{-d}. \tag{11}$$

In the presence of ΔA_{+d} and ΔA_{-d}, the measured overlay, OV_m, is obtained using

$$\mathrm{OV}_m = d \cdot \frac{(A_{+d} + A_{-d})}{(A_{+d} - A_{-d})} = d \cdot \frac{2K\mathrm{OV} + (\Delta A_{+d} + \Delta A_{-d})}{2Kd + (\Delta A_{+d} - \Delta A_{-d})} = d \cdot \frac{2K\mathrm{OV} + 2\Delta A_m}{2Kd + 2\Delta A_d}. \tag{12}$$

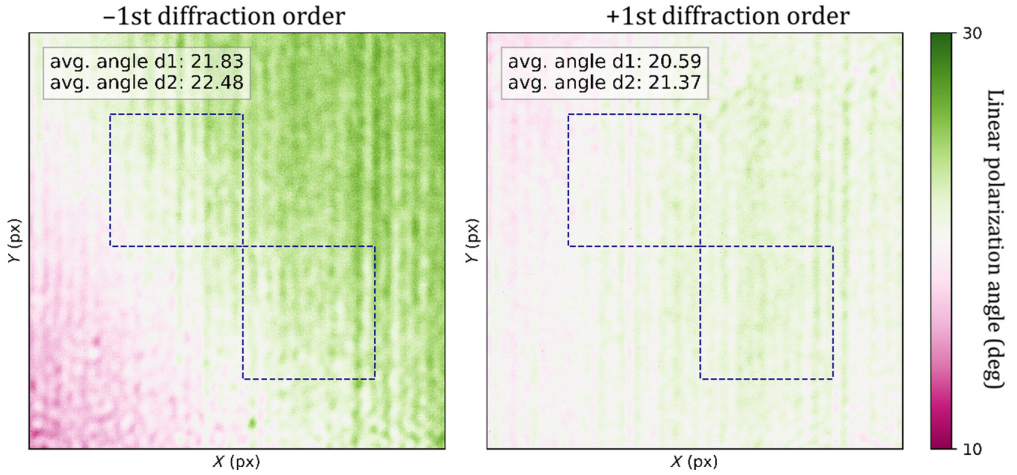

Fig. 8 Linear polarization angle for the incoming illumination beams measured on a large calibration grating with a uniform response. The dotted blue lines sketch the outline of the grating pads of a DBO target. The average angle over the region of interest of the grating pads is stated in the top left corner.

Here, the terms $\Delta A_m = \frac{(\Delta A_{+d} + \Delta A_{-d})}{2}$ and $\Delta A_d = \frac{(\Delta A_{+d} - \Delta A_{-d})}{2}$ are, respectively, the mean and the differential asymmetry of the sensor. Normally, these sensor-induced asymmetries are small, and the retrieved overlay can be approximated as

$$\mathrm{OV}_m = \mathrm{OV}\left(1 - \frac{\Delta A_d}{Kd}\right) + \frac{\Delta A_m}{Kd}. \tag{13}$$

Equation (13) shows that differential asymmetries can introduce a scaling error and offset in the DBO overlay measurements.

To further investigate the effect of differential sensor asymmetry in our microscope, the signal values A_{+d} and A_{-d} are plotted in Fig. 9 as a function of the programmed overlay $+d$. From Fig. 9, it can be observed that A_{+d} and A_{-d} scale linearly with the programmed $\mathrm{OV} + d$ and that there are small asymmetry offsets for the different pads. We can retrieve the individual asymmetry offsets by fitting a linear function through the signal slopes in Fig. 9.

By correcting the asymmetry in the signals using the retrieved offsets, we calculate the corresponding overlay, as shown in Fig. 10. The asymmetry-corrected OV curves exhibit slopes and offsets that closely align with the theoretical values of 1 and 0, respectively. This suggests that the deviations in slopes and offsets observed in Fig. 10 of the main text are likely due to the differential asymmetry of the illumination polarization state.

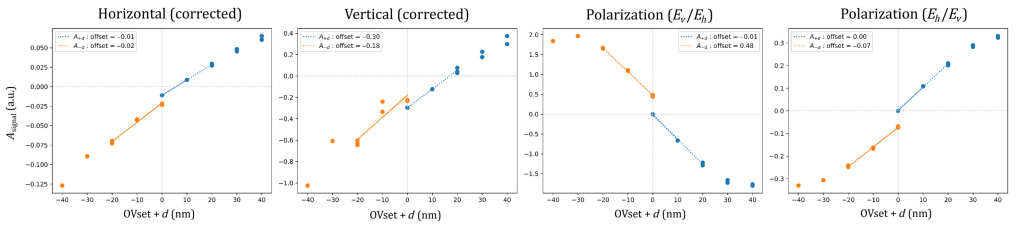

Fig. 9 Asymmetry signals, $A_{\pm d}$, for the individual $+d$ and $-d$ pads of a diffraction-based overlay target as a function of the programmed overlay $+d$. The A_{+d} (blue) and A_{-d} (orange) signals scale linearly and have an individual offset.

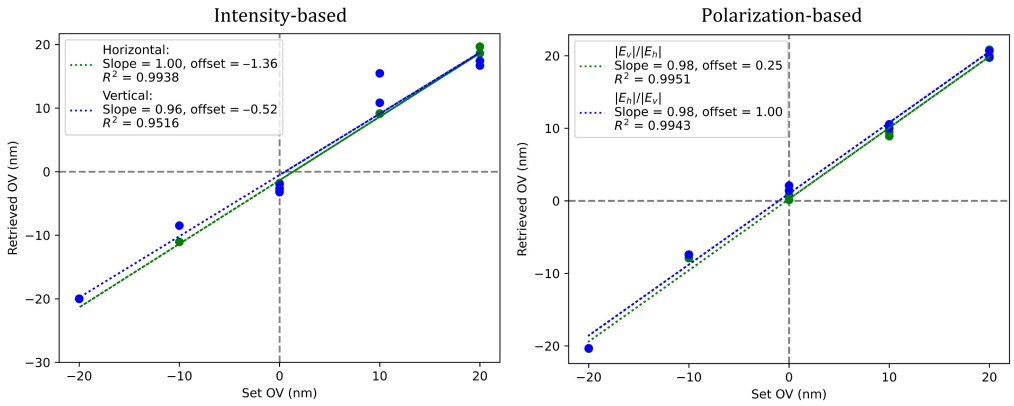

Fig. 10 Asymmetry-corrected retrieved OV plotted as a function of the programmed OV of multiple diffraction-based overlay targets. The dotted lines depict linear fit through the data points, from which the slope and offset of the OV curves are extracted.

Disclosures

The authors declare no conflicts of interest. The authors declare that they have patents or patent applications. Marc Noordam and Arie den Boef are employees of ASML.

Code and Data Availability

Data underlying the results presented in this paper are not publicly available at this time but may be obtained from the authors upon reasonable request.

Acknowledgments

The authors thank Tamar Cromwijk, Manashee Adhikary, Mohamed Abdelkhalik Mohamed, Bartjan Spaanderman, Johannes F. de Boer, Dierck Hillmann, and Simon Mathijssen for their valuable contributions and support for this research. This work was conducted at the Advanced Research Center for Nanolithography, a public–private partnership between the University of Amsterdam, Vrije Universiteit Amsterdam, Rijksuniversiteit Groningen, the Netherlands Organization for Scientifc Research (NWO), and the semiconductor-equipment manufacturer ASML. We thank ASML for providing the DBO calibration targets used in this paper. ChatGPT was used for language and grammar clean-up.

References

1. W. Yang et al., "Novel diffraction-based spectroscopic method for overlay metrology," *Proc. SPIE* **5038**, 200–207 (2003).
2. K. Bhattacharyya et al., "Multi-wavelength approach towards on-product overlay accuracy and robustness," *Proc. SPIE* **10585**, 105851F (2018).
3. M. Adel et al., "Diffraction order control in overlay metrology: a review of the roadmap options," *Proc. SPIE* **6922**, 692202 (2008).
4. P. Leray et al., "Diffraction based overlay metrology: accuracy and performance on front end stack," *Proc. SPIE* **6922**, 69220O (2008).
5. A. J. den Boef, "Optical wafer metrology sensors for process-robust cd and overlay control in semiconductor device manufacturing," *Surf. Topogr. Metrol. Prop.* **4**, 023001 (2016).
6. E. Cuche, F. Bevilacqua, and C. Depeursinge, "Digital holography for quantitative phase-contrast imaging," *Opt. Lett.* **24**(5), 291–293 (1999).
7. F. Dubois and P. Grosfils, "Dark-field digital holographic microscopy to investigate objects that are nano-sized or smaller than the optical resolution," *Opt. Lett.* **33**(22), 2605–2607 (2008).
8. C. Messinis et al., "Diffraction-based overlay metrology using angular-multiplexed acquisition of dark-field digital holograms," *Opt. Express* **28**, 37419–37435 (2020).
9. T. T. M. van Schaijk et al., "Diffraction-based overlay metrology from visible to infrared wavelengths using a single sensor," *J. Micro/Nanopattern. Mater. Metrol.* **21**, 014001 (2022).

10. C. Messinis et al., "Aberration calibration and correction with nano-scatterers in digital holographic microscopy for semiconductor metrology," *Opt. Express* **29**(23), 38237–38256 (2021).
11. T. van Gardingen-Cromwijk et al., "Field-position dependent apodization in dark-field digital holographic microscopy for semiconductor metrology," *Opt. Express* **31**, 411–425 (2022).
12. M. Adhikary et al., "Illumination spot profile correction in digital holographic microscopy for overlay metrology," *J. Micro/Nanopattern. Mater. Metrol.* **22**, 024001 (2023).
13. X. Chen et al., "Multi-spectral snapshot diffraction-based overlay metrology," *Opt. Letters* **48**, 3383–3386 (2023).
14. C. Fallet et al., "Overlay measurements by Mueller polarimetry in back focal plane," *J. Micro/Nanolithogr. MEMS MOEMS* **10**(3), 033017 (2011).
15. T. Colomb et al., "Polarization microscopy by use of digital holography: application to optical-fiber birefringence measurements," *Appl. Opt.* **44**, 4461–4469 (2005).
16. H. Liu et al., "Real-time Jones matrix synthesis by compact polarization inline holographic microscopy," *Laser Photonics Rev.* **18**, 2301261 (2024).
17. Y. Kim et al., "Polarization holographic microscopy for extracting spatio-temporally resolved Jones matrix," *Opt. Express* **20**(9), 9948–9955 (2012).
18. G. Coppola and M. A. Ferrara, "Polarization-sensitive digital holographic imaging for characterization of microscopic samples: recent advances and perspectives," *Appl. Sci.* **10**(13), 4520 (2020).
19. C. Messinis et al., "Impact of coherence length on the field of view in dark-field holographic microscopy for semiconductor metrology: theoretical and experimental comparisons," *Appl. Opt.* **59**(11), 3498–3507 (2020).
20. T. van Gardingen-Cromwijk et al., "Computational vibration mitigation using phase interpolation in digital holographic microscopy for overlay metrology," *Opt. Express* **32**(21), 36315–36328 (2024).

Marc Noordam received his PhD in experimental physics from the Delft University of Technology in 2023, where he focused on nanophotonics in 2D materials and plasmonic systems. Currently, he is a postdoctoral researcher at ARCNL, developing novel microscopy systems for OV metrology.

Tamar van Gardingen-Cromwijk is currently a PhD candidate at the Advanced Research Center for Nanolithography (ARCNL) in Amsterdam, and the Vrije Universiteit, Amsterdam. She received her BSc and MSc degrees in applied physics from the Eindhoven University of Technology in 2019 and 2021, respectively. The goal of her PhD research is the development of a metrology tool based on digital holography, capable of robust semiconductor metrology with the aid of computational algorithms.

Arie den Boef received his degree in electrical engineering from the Eindhoven Polytechnic Institute and his PhD from the University of Twente. He worked at Philips from 1979 to 1997 where he worked in the area of laser diodes, optics, MRI, and optical storage. He joined ASML in 1997, where he explored various optical metrology techniques. He is also a part-time full professor at the Vrije Universiteit of Amsterdam and leads the group of Computational Imaging at ARCNL.